RSC Advances

This is an *Accepted Manuscript*, which has been through the Royal Society of Chemistry peer review process and has been accepted for publication.

Accepted Manuscripts are published online shortly after acceptance, before technical editing, formatting and proof reading. Using this free service, authors can make their results available to the community, in citable form, before we publish the edited article. This *Accepted Manuscript* will be replaced by the edited, formatted and paginated article as soon as this is available.

You can find more information about *Accepted Manuscripts* in the Information for Authors.

Please note that technical editing may introduce minor changes to the text and/or graphics, which may alter content. The journal's standard Terms & Conditions and the Ethical guidelines still apply. In no event shall the Royal Society of Chemistry be held responsible for any errors or omissions in this *Accepted Manuscript* or any consequences arising from the use of any information it contains.

ROYAL SOCIETY OF CHEMISTRY

www.rsc.org/advances

Cite this: DOI: 10.1039/c0xx00000x

www.rsc.org/xxxxxx

ARTICLE TYPE

Hierarchical Silicon Nanostructured Arrays via Metal-Assisted Chemical Etching

Hao Lin,[a,†] Ming Fang,[a,†] Ho-Yuen Cheung,[b] Fei Xiu,[a,d] SenPo Yip,[a,d] Chun-Yuen Wong,[b] Johnny C. Ho*[a,c,d]

Received (in XXX, XXX) Xth XXXXXXXXX 20XX, Accepted Xth XXXXXXXXX 20XX
DOI: 10.1039/b000000x

Hierarchically arranged nanostructures, configured in both nanopillars and nanoholes, have been fabricated via a low-cost approach that combines metal-assisted chemical etching (MaCE), nanosphere and conventional lithography. By manipulating the catalyst morphology as well as the deposition method, different interesting nanostructures like nanowalls and nanograsses were fabricated at the galleries among the nanopillar blocks. Using the similar strategy, hierarchical negative structures (nanoholes) have also been successfully demonstrated. The successful constructions of these diversified hierarchical nanostructures illustrates that MaCE could be deployed as a feasible, low-cost method for multi-scale silicon micro/nano machining, which is highly desirable for widespread applications including tissue engineering, optoelectronics, photonic devices and lab-on-chip systems.

Introduction

Hierarchical micro/nano structures possess unique interfacial properties for wetting, adhesion, thermal management, electrical conduction and light trapping, in which these properties can work synergistically and offer superior material/device performances, being of great interest for widespread applications such as optoelectronics [1,2], photonic devices [3–6], bio-/chemical-sensors [7–9], biomedicine [10,11] and so on. Usually, these structures could be fabricated by employing electron-beam lithography (EBL), focused-ion-beam lithography (FIB) and reactive-ion etching (RIE) for patterning and/or etching. However, these techniques are only suitable for small-area fabrications owing to the high cost and low through-put, which has severely retarded the practical applications of these hierarchical materials. In recent years, wet chemical etching methods have also been actively explored for fabrications of high-aspect-ratio silicon-based nanostructures, well known as electrochemical micromachining (ECM) [12,13] and metal-assisted chemical etching (MaCE) [14–16]. Comparing with the standard dry etching methods, wet etching techniques hold several key advantages here including the low fabrication cost, eliminated surface damages and more importantly, the achievable high structural aspect-ratios. For instance, a recent report by Chang and Sakdinawat showed that high-resolution Si nanostructures (e.g., nanowalls with 32 nm of the width, 136 nm of the period and 2.5 μm of the height) could be formed by MaCE for applications in hard X-ray diffractive optics.[17] Moreover, combining MaCE with the low-cost nanosphere lithography, highly ordered silicon nanopillar, nanopencil and nanocone arrays have been successfully fabricated in a controllable manner.[18,19] Nevertheless, although MaCE has been successfully employed for fabrications of uniformly distributed Si nanostructures, it is still rarely utilized to obtain hierarchical micro/nano structures.

Here, we report the fabrication of hierarchically arranged nanostructures, in the configuration of both pillars and holes, by MaCE coupled with polystyrene (PS) nanospheres as well as conventional lithography. By manipulating the catalyst deposition methods and etching conditions, we can attain diversified hierarchical micro/nano structures, which demonstrate that MaCE could be employed as a feasible and low-cost method to achieve various large-area hierarchical micro/nano structures for technological utilization.

Experimental

Single-crystalline p-type (100) Si wafers were used for fabrications of the hierarchical silicon micro/nano structures. Metal films were deposited through electron-beam evaporation at a rate of 1~2 Å/s. Photolithography was carried out in a class 100 cleanroom employing a MA/BA6 mask aligner (Karl Suss) and AZ 5214E photoresist (Micro-Chemicals). Monodispersed PS nanospheres were purchased from Microparticles Gmbh. Closely packed PS nanosphere monolayers were obtained by assembling the spheres on water surface through the Langmuir–Blodgett (LB) method and transferred on to the target wafers. The assembled nanospheres were shrunk by oxygen plasma etching and used as deposition or etching masks for the subsequent metal patterning. To conduct the MaCE, the silicon wafers with patterned catalyst were immersed in HF/H_2O_2 (4.8M, 0.2M) aqueous solutions at room temperature for 20~60 min in dark. After the etching, the Au catalyst was removed using aqua regia solution (HNO_3/HCl, 1:3 in volume).

Results and Discussion

RSC Advances Accepted Manuscript

The MaCE of silicon typically takes place in a system which contains silicon wafers, metal catalysts (Ag, Au, or Pt) and an etchant solution (HF and H_2O_2 mixtures). The etching process in principle is chemical reduction/oxidation reactions occurring at the metal-Si interface [14,16]. The oxidants, such as H_2O_2, are reduced to water by taking electrons from the metal catalyst, leaving holes in the metal. The holes would further get injected into the silicon and causes oxidizations of the interfacial silicon. The oxidized silicon is then dissolved by HF, leading to forward movement of the metal catalyst, and thus, this catalyzed etching could take place continuously. Because of this above-mentioned etching mechanism, the cross-sectional shape of the etched structures is basically determined by the pattern of the metal catalyst. Therefore, employing metal nanomesh and nanodisk as the catalyst, various silicon nanostructures, including nanopillars and nanoholes could be obtained (Supporting Information Figure S1). As the etching reaction mainly occurs at the metal-silicon interface, high-aspect ratio nanostructures could be obtained accordingly with the proper control in the etching condition.

In order to obtain hierarchical or patterned nanopillar arrays, we first fabricated patterned metal nanomeshes on silicon surface by combining nanosphere and conventional lithography. It is known that Ag and Au are the most commonly used catalysts in MaCE. In this work, we decide to select Au as the catalyst here, since it has been demonstrated with the better film stability than Ag in the etching solution, in which this stability is highly crucial to achieve the smooth etched surface.[20–22] In general, we can obtain Au mesh patterns through three different deposition methods by changing the sequence of the two lithographic processes, namely type I, type II and type III as illustrated in Figure 1a-c (see Supporting Information Figure S2 for details). After the catalyst deposition, the silicon chips were then submerged in a HF/H_2O_2 solution to undergo MaCE. During the process, the silicon underneath the metal film (catalyst) got etched, leaving the uncovered regions as nanopillars after the etching process (Figure 1d).

In predictions, the patterned regions (continuous metal films) would generate structures with smooth side walls and flat backgrounds after etching. However, our experimental results reveal that the three catalyst patterns with different deposition sequence (i.e. type I, II or III) could give significantly distinct morphologies, and none of them leaded to a flat background (Figure 2). Specifically, when using the type I Au catalyst film (Figure 1a), a ridge was formed under the continuous metal film (Figure 2a). It is obvious that the reaction rate at the center region (without any pattern) was much lower than that at the edge region (with patterns), which caused this non-flat etching background. In the second case, where type II Au patterns (Figure 1b) were used as the catalyst, the morphology obtained was very close to the expectation; in any case, a closer look would disclose that there are continuous silicon walls at the edges of the micro patterns, and simultaneous, the etching depth of the patterned regions were slightly smaller than that of the meshed regions (Figure 2b). Finally, when using type III Au catalyst patterns, very thin grass-like nanostructures are appeared among the regular pillar arrays (Figure 2c), which is somewhat different to the morphologies obtained in the first two cases. At the same time, it is noted that there is not any noticeable difference of the etching depth observed over different regions here.

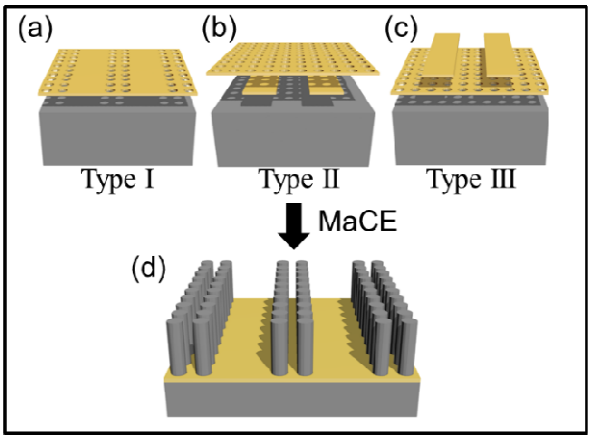

Figure 1. Schematic illustration of the fabrication of patterned nanopillar arrays via the metal-assisted wet etching. (a),(b) and (c) are gold nanomeshes (catalyst) fabricated with three different patterning methods and (d) represents obtained hierarchical nanostructures after the MaCE process.

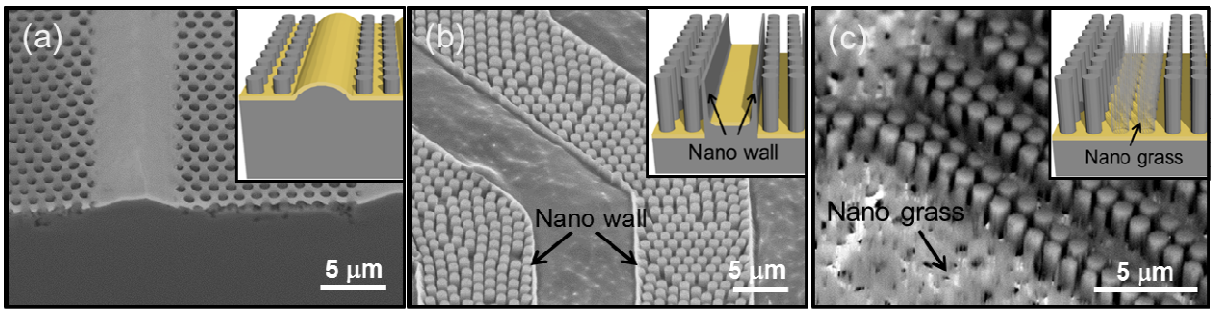

Figure 2. SEM images of nanostructures obtained after MaCE using (a) type I, (b) type II and (c) type III catalyst patterns. The insets show the schematic illustration of the corresponding structures.

In wet chemistry, it is known that the sufficient liquid exchange is extremely important to achieve uniform reaction rate. In MaCE, the metal (Au here) serves as a catalyst for the reaction between silicon and the H_2O_2/HF mixture; however, large-area coverage of the metal film could also hinder the liquid exchange at the center area (Figure 3a, b), which eventually leads to degraded reaction rate. As a result, a ridge-like microstructure was produced in cases of the type I Au catalyst pattern (Figure 2a).

RSC Advances Accepted Manuscript

This journal is © The Royal Society of Chemistry [year]

Nevertheless, this structure was not attained when type II and type III catalyst films were used. Notably, since both type II and type III catalyst films were patterned through two-step deposition methods, in this case, it is likely to form boundary defects/cracks between the two deposited layers (Figure 3c1, d1). As presented in Figure 3c, lateral cracks are appeared between the first and the second metal layer, especially when the first-deposited metal patterns have titled edges (induced by the slopped photoresist edges). Consequently, the second metal layer tends to dissociate from the first layer during the etching due the stress induced by the different etching speed. This way, the meshed region was etched much faster due to better solution exchanges. On the contrary, the continuous covered region showed a slower etching rate. Actually, further manipulating the pattern to a larger dimension, the etching rate over the micropatterns were also degraded with a distribution, being slower at the middle and faster at the edges, depending on the liquid exchange ability and pattern size (Supporting Information Figures S3). Due to the deteriorated etching rate, the cracked metal film was not able to fully cover the etched silicon surface when the etching is progressed further because of the increased surface area. The uncovered regions would be eventually evolved into continuous nanowalls as depicted in the obtained samples (Figure 2b). Similarly, in the type III metal patterns, there was also a tendency to form tiny cracks between the two deposited metal layers at the hole edges of the nanomesh, as illustrated in Figure 3d. On the one hand, these cracks can favor the solution exchange and thus yield a more uniform etching rate over the entire catalyst covered region; on the other hand, they can also result in the incomplete etching of designed structures, forming arrays of nano-grasses (Figure 2c). Importantly, all these different thickness selection of the two metal layers can as well influence the morphology of the nanograsses. It seems that when the second metal layer is thinner than the first metal layer, the obtained nanograsses were thicker in the diameter (Supporting Information Figure S4a, b), which was presumably resulted from the larger cracks due to the insufficiently metal filling-up into the holes of the first mesh layer. In contrast, when the second metal layer got thicker than the first layer, there were only very small cracks existed in the metal film at the micro-patterned area, and the nanograss would become thin and sparsely distributed (Supporting Information Figure S4c). Meanwhile, as the liquid exchange ability at some locations were severely decreased due to the coverage of the second metal layer, the etching rate turned out to be varied over different locations and the etching interface become uneven, leading to crumpled metal film and decreased cross-sectional etching area. As a result, the nanopillar blocks get tapered. With these structures obtained from above, we can further control their morphologies by applying the catalyst-free isotropic/anisotropic chemical etching. For instance, by immersing the type III catalyst derived samples in a KOH solution at 90 ^{o}C, we can remove the nanograss and achieve various hierarchically configured, high-aspect-ratio nanopillar arrays as shown in Figure 4.

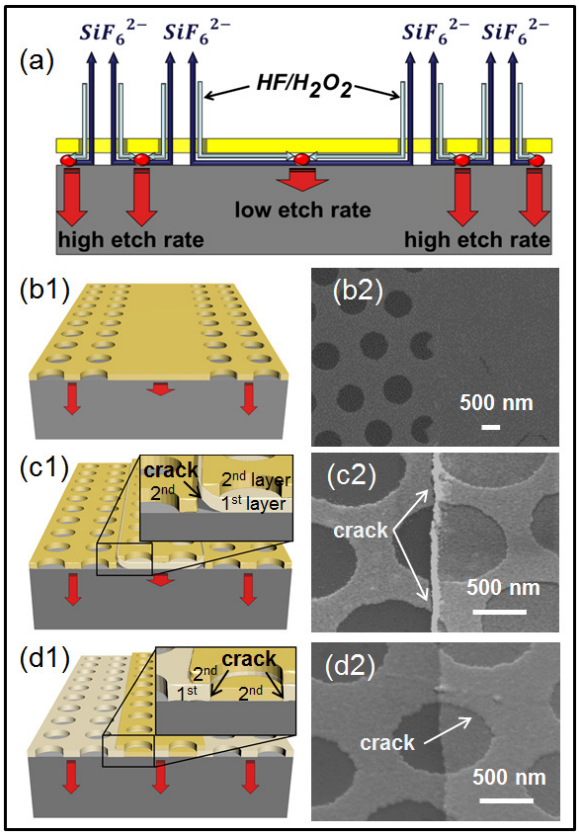

Figure 3. (a) Schematic illustration showing the different etching rates due to the different solution permeability at different locations. (b), (c), (d) Schematic illustrations and SEM images showing the crack formations in type I, type II and type III catalyst patterns, respectively.

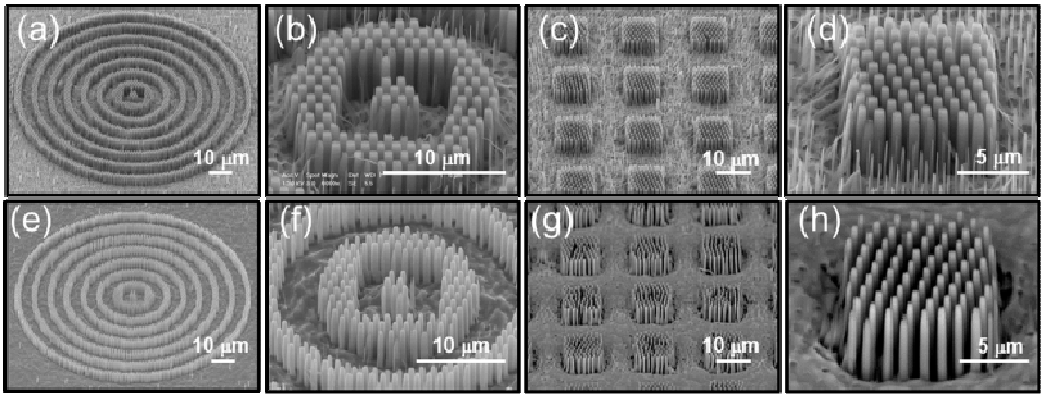

Figure 4. SEM images of various hierarchical nanostructures before (a-d) and after (e-h) removal of the nanograss.

RSC Advances Accepted Manuscript

Cite this: DOI: 10.1039/c0xx00000x

www.rsc.org/xxxxxx

ARTICLE TYPE

In addition to positive nanostructures, nanohole-based negative hierarchical nanostructures could also be useful for many applications. In order to fabricate these negative structures, patterned Au nanodisk arrays were fabricated as the catalyst on silicon. These Au nanodisks can be obtained by utilizing Ar plasma etching/sputtering with PS nanospheres as the etching masks [23–25]. To integrate micro-scale patterns into the disk arrays, we first fabricated a thin layer of Cr micropatterns on the silicon wafer using the conventional photolithography before the deposition of the Au film (Figure 5a). As Cr is durable to the Ar plasma, it can keep intact during the Au disk fabrication. Also, Cr is inactive in MaCE, it can serve as a blocking layer for the anisotropic etching. Then, the sample was put in the HF/H_2O_2 etchant solution, and the Au disks which were not covered by Cr could initiate the chemical etching and yield nanohole structures (Figure 5b). Finally, the Cr and Au could be completely removed, leaving hierarchical nanohole arrays with the very smooth surface. All these nanostructures could be used as replica modes to fabricate inverted hierarchical nanostructures, and the smooth surface could be advantageous for the release of the replicated layer.

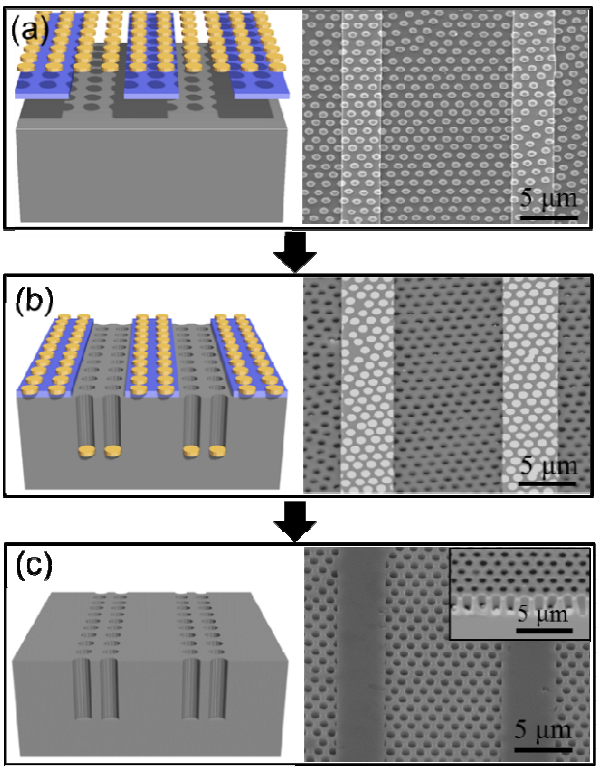

Figure 5. Fabrications of hierarchical negative nanostructures. (a) Deposition of Au nanodisk arrays on a (100) silicon surface with Cr micropatterns, (b) after MaCE and (c) obtaining patterned nanohole arrays after the Cr and Au removal.

Conclusions

In conclusion, we present a low-cost approach to fabricate hierarchical arranged silicon nanostructures by combining MaCE with nanosphere and conventional lithography. Through controllable depositions of the metal catalyst films, we can achieve different interesting nanostructures like nanowalls and nanograsses at predefined positions among nanopillar arrays. We have also successfully fabricated hierarchical negative structures by changing the catalyst shape. Moreover, the morphology of obtained nanostructures could be further manipulated by employing isotropic chemical etching. All these micro/nano hierarchical silicon structures can provide interesting platforms to explore the interplay between the structures and the biological cell attachment behavior and may also find fascinating applications in optoelectronics, photonic devices and bulk lab-on-chip systems.

Acknowledgements

This research was financially supported by the City University of Hong Kong (Project No. 9667086), the National Natural Science Foundation of China (Grant Number 51202205), the Guangdong National Science Foundation (Grant Number S2012010010725), the Science Technology and Innovation Committee of Shenzhen Municipality (Grant Number JCYJ20120618140624228), and was supported by a grant from the Shenzhen Research Institute, City University of Hong Kong.

Notes and references

[a] *Department of Physics and Materials Science, City University of Hong Kong, 83 Tat Chee Avenue, Kowloon Tong, Kowloon, Hong Kong*
[b] *Department of Biology and Chemistry, City University of Hong Kong, 83 Tat Chee Avenue, Kowloon Tong, Kowloon, Hong Kong*
[c] *Centre for Functional Photonics (CFP), City University of Hong Kong, 83 Tat Chee Avenue, Kowloon Tong, Kowloon, Hong Kong*
[d] *Shenzhen Research Institute, City University of Hong Kong, Shenzhen, China*
† *These authors contributed equally to this work.*
Corresponding author:
Electronic mail: johnnyho@cityu.edu.hk

1. S. Jeong, E. C. Garnett, S. Wang, Z. Yu, S. Fan, M. L. Brongersma, M. D. McGehee, and Y. Cui, Nano Lett., 2012, 12, 2971–6.
2. W.-R. Wei, M.-L. Tsai, S.-T. Ho, S.-H. Tai, C.-R. Ho, S.-H. Tsai, C.-W. Liu, R.-J. Chung, and J.-H. He, Nano Lett., 2013, 13, 3658–63.
3. B.-S. Song, S. Noda, T. Asano, and Y. Akahane, Nat. Mater., 2005, 4, 207–210.
4. B. Corcoran, C. Monat, C. Grillet, D. J. Moss, B. J. Eggleton, T. P. White, L. O'Faolain, and T. F. Krauss, Nat. Photonics, 2009, 3, 206–210.
5. A. Shakoor, R. Lo Savio, P. Cardile, S. L. Portalupi, D. Gerace, K. Welna, S. Boninelli, G. Franzò, F. Priolo, T. F. Krauss, M. Galli, and L. O'Faolain, Laser Photon. Rev., 2013, 7, 114–121.

RSC Advances Accepted Manuscript

6. F. Priolo, T. Gregorkiewicz, M. Galli, and T. F. Krauss, Nat. Nanotechnol., 2014, 9, 19–32.
7. R. A. Potyrailo, H. Ghiradella, A. Vertiatchikh, K. Dovidenko, J. R. Cournoyer, and E. Olson, Nat. Photonics, 2007, 1, 123–128.
8. S. Y. Kim, J. Yu, S. J. Son, and J. Min, Ultramicroscopy, 2010, 110, 659–65.
9. K. Kuwabara, M. Ogino, T. Ando, and A. Miyauchi, Appl. Phys. Lett., 2008, 93, 033904.
10. J. Tan and W. M. Saltzman, Biomaterials, 2004, 25, 3593–601.
11. A. Ranella, M. Barberoglou, S. Bakogianni, C. Fotakis, and E. Stratakis, Acta Biomater., 2010, 6, 2711–20.
12. M. Bassu, S. Surdo, L. M. Strambini, and G. Barillaro, Adv. Funct. Mater., 2012, 22, 1222–1228.
13. G. Polito, S. Surdo, V. Robbiano, G. Tregnago, F. Cacialli, and G. Barillaro, Adv. Opt. Mater., 2013, 1, 894–898.
14. X. Li and P. W. Bohn, Appl. Phys. Lett., 2000, 77, 2572.
15. X. Li, Curr. Opin. Solid State Mater. Sci., 2012, 16, 71–81.
16. Z. Huang, N. Geyer, P. Werner, J. de Boor, and U. Gösele, Adv. Mater., 2011, 23, 285–308.
17. C. Chang and A. Sakdinawat, Nat. Commun., 2014, 5, 4243.
18. H. Lin, H.-Y. Cheung, F. Xiu, F. Wang, S. Yip, N. Han, T. Hung, J. Zhou, J. C. Ho, and C.-Y. Wong, J. Mater. Chem. A, 2013, 1, 9942.
19. H. Lin, F. Xiu, M. Fang, S. Yip, and H. Cheung, ACS Nano, 2014, 8, 3752–3760.
20. H. Han, Z. Huang, and W. Lee, Nano Today, 2014, 9, 271–304.
21. J. Kim, H. Han, Y. H. Kim, S.-H. Choi, J.-C. Kim, and W. Lee, ACS Nano, 2011, 5, 3222–9.
22. J. Kim, Y. H. Kim, S.-H. Choi, and W. Lee, ACS Nano, 2011, 5, 5242–8.
23. P. Hanarp, M. Käll, and D. Sutherland, J. Phys. Chem. B, 2003, 107, 5768–5772.
24. Y. B. Zheng, B. K. Juluri, X. Mao, T. R. Walker, and T. J. Huang, J. Appl. Phys., 2008, 103, 014308.
25. F. Liu, M. M. Wong, S. Chiu, H. Lin, J. C. Ho, and S. W. Pang, Biosens. Bioelectron., 2014, 55, 141–148.

RSC Advances Accepted Manuscript